energies

MDPI

Article

Circular Valorization of Waste PET into Ni-BDC Metal-Organic Frameworks for Advanced and Sustainable Energy Storage Applications

Deeptiman Dutta [1], Jan Taler [2], Monika Piwowarczyk [2], Dawid Taler [3], Parthasarathy Rajesh Kanna [1], Sunilkumar Dhakshinamoorthy [4] and Ranjitha Jambulingam [4,*]

[1] School of Mechanical Engineering, Vellore Institute of Technology, Vellore 632014, India
[2] Department of Energy, Cracow University of Technology, al. Jana Pawła II 37, 31-864 Kraków, Poland
[3] Department of Thermal Processes, Air Protection and Waste Management, Cracow University of Technology, al. Jana Pawła II 37, 31-864 Kraków, Poland
[4] CO_2 Research and Green Technologies Centre, Vellore Institute of Technology, Vellore 632014, India
* Correspondence: jranji16@gmail.com

Abstract

Growing environmental concerns and the rapid depletion of fossil fuels have accelerated the need for sustainable energy storage systems. This research reports converting waste polyethylene terephthalate (PET) into terephthalic acid (BDC) and then using it as an organic linker to synthesize a nickel-coordinated metal-organic framework (Ni-BDC) for supercapacitor applications. The BDC ligands extracted from PET via alkaline hydrolysis were analyzed to confirm their structural and crystalline properties with commercial terephthalic acid. Using a simple one-step co-precipitation method, the Ni-BDC MOF was synthesized and characterized using UV–Visible spectroscopy, Fourier-Infrared spectroscopy, X-ray diffraction, Raman spectroscopy, Field-emission scanning electron microscopy, X-ray photoelectron spectroscopy (XPS), and Brunauer–Emmett–Teller (BET) surface area analysis. These characterization results confirmed the formation of a highly crystalline coordination framework with bidentate carboxylate bridging between Ni^{2+} ions and PET-derived ligands. The electrochemical performance was evaluated in 1 M KOH electrolyte using a three-electrode and a symmetric two-electrode configuration. In the three-electrode configuration, the Ni-BDC electrode showed a maximum specific capacitance of 1118 F g^{-1} at a current density of 1 A g^{-1}, which decreased to 129 F g^{-1} at 10 A g^{-1}. Electrochemical impedance spectroscopy revealed a solution resistance (R_s) of 3.6 Ω, while the inclined Nyquist response indicated non-ideal capacitive characteristics. Furthermore, the symmetric two-electrode device exhibited specific capacitances of 36.36 and 4.83 F g^{-1} at current densities of 0.5 and 10 A g^{-1}, respectively. The device retained 67% of its capacitance after 8000 galvanostatic charge-discharge cycles at 15 A g^{-1}, with a coulombic efficiency of approximately 100.1%. These findings demonstrate the feasibility of using waste PET-derived terephthalic acid to develop functional Ni-BDC electrode materials and offer a potential pathway to integrate plastic waste valorization with electrochemical energy storage applications.

Keywords: Energy storage performance; Ni-BDC MOF; PET-derived ligands; supercapacitor applications

Check for updates

Academic Editor: Georg Frey

Received: 19 September 2026
Revised: 29 October 2026
Accepted: 4 November 2026
Published: 16 November 2026

Copyright: © 2026 by the authors. Licensee MDPI, Basel, Switzerland. This article is an open access article distributed under the terms and conditions of the Creative Commons Attribution (CC BY) license.

1. Introduction

Rapidly increasing global energy demand, driven by industrialization, urbanization, and population growth, has placed tremendous strain on available energy resources [1,2].

Conventional energy sources, largely fossil-fuel-based, face limited supply and pose major environmental challenges [3,4]. Solar and wind power offer feasible alternatives to conventional non-renewable energy sources. Still, their intermittency, unpredictability, limited availability, and sustainability concerns drive the development of efficient, effective energy storage devices [5,6]. Electrochemical energy storage systems, such as batteries, are important components of future energy systems [7]. Among energy storage systems, supercapacitors, also known as electrochemical capacitors, have attracted significant research attention due to their high power density, ultra-fast charge and discharge rates, long lifespan, and high safety [8,9]. Supercapacitors can bridge the performance gap between dielectric capacitors and the energy-storage capabilities of Li-ion batteries [10]. The supercapacitor comprises four key components: the current collector, the electrode, the electrolyte, and the separator [11]. The electrode is the most critical factor in determining the supercapacitor's electrochemical performance, including capacitance per unit, rate performance, energy density, and long-term cycling stability [12,13]. Much research has focused on designing supercapacitor electrode materials, including carbon materials, transition metal oxides/hydroxides, conductive polymers, and composites of these materials [14–16]. However, these materials have intrinsic limitations, including limited active sites, limited ion access, structural changes, and poor electrical conductivity [17]. Metal–Organic Frameworks (MOFs) are a promising, sustainable alternative for supercapacitor electrodes [18,19]. MOFs are crystalline nanoporous materials made of metal ions or metal clusters and coordinated organic ligands [20]. Recent developments have shown promising results for MOFs as potential supercapacitor electrodes [21]. This is due to the framework's unusual characteristics, including an exceptionally large specific surface area, a crystalline pore structure, and the ability to modify pore diameters and chemical composition [22,23]. However, despite these advantages, crystalline MOFs also exhibit poor intrinsic electrical conductivity and limited electrochemical stability, which significantly limit their direct applicability as supercapacitors [24]. To address these challenges, researchers have proposed several strategies, including metal-ion control, ligand modification, composite formation, and structural modification. In summary, changing the metal center and the organic ligand remains one of the most important ways to improve MOF electrochemical performance, as these changes directly affect structure and properties [25]. The choice of metal ion is particularly important, especially when compared with extensively researched metals such as nickel [26], cobalt [27], and manganese [28]. Among these metal ions, nickel has attracted considerable interest for electrochemical energy-storage applications because of its accessible redox chemistry and the reversible Ni^{2+}/Ni^{3+} redox process in alkaline electrolytes [29]. Nickel-containing coordination materials have therefore been investigated as electrochemically active electrode materials for supercapacitors [30]. In addition, coordinating Ni^{2+} with aromatic carboxylate ligands offers an opportunity to construct structurally defined metal-organic frameworks with electrochemically active metal centers [31]. Aromatic carboxylic acids are widely used in the synthesis of MOFs because of their high affinity, rigidity, and chemical stability towards the metal centers of the framework [32]. The acidity of benzene ring-containing dicarboxylic acids offers considerable benefits for designing specific MOF topologies and controlling framework porosity, including the potential to deliver robust architectures [33]. Electron delocalization in conjugated systems plays a critical role in enhancing charge transport within the framework. Recently, attention has increasingly focused on using waste-derived organic molecules as MOF precursors because these approaches can convert post-consumer waste into functional chemical building blocks. In this context, waste PET is particularly interesting because its polymer backbone contains terephthalate units that can be chemically recovered and subsequently utilized as organic linkers in coordination materials. This study therefore investigates PET-derived terephthalic acid as

a precursor for Ni-BDC formation and evaluates the resulting material for electrochemical energy-storage applications [34]. Among plastic wastes, polyethylene terephthalate (PET) is the most widely utilized [35]. As a result, enormous quantities of non-biodegradable waste are being disposed of worldwide. Chemical recycling is an alternative approach to valorize waste PET by recovering terephthalic acid (TPA), which can be used as an organic linker for metal–organic framework (MOF) synthesis. Although traditional mechanical recycling is a major pathway for managing PET waste, using recovered TPA as a functional precursor offers an opportunity to convert plastic waste into value-added materials for specific applications, such as energy storage. The aromatic dicarboxylate ligands derived from PET offer several advantages for MOF based supercapacitor electrodes. The presence of a benzene ring in these ligands imparts stability to the ligands. The dicarboxylate functionality allows strong coordination to the metal center [36]. The molecular structures of PET derived ligands are flexible, which influences conjugation length, pore environment, dimensionality, and overall electrochemistry [37,38]. The electrochemical properties of the resulting Ni-BDC material are an important aspect to explore, particularly in relation to the structural characteristics of the recovered ligand and its pseudocapacitive behavior, while terephthalic acid from PET has been explored as a precursor for metal organic frameworks. Thus, this work is focused on the synthesis, structural characterization and electrochemical evaluation of Ni-BDC from terephthalic acid recovered from post-consumer PET. This research focuses on the synergistic combination of eco-friendly metal ions and recycled organic linkers to produce MOFs with high porosity, structural robustness, and improved electrolyte accessibility. Nickel-based PET-derived aromatic dicarboxylate ligand MOFs were synthesized using a simple one-step co-precipitation method. The structural, morphological, and electrochemical properties of the prepared Ni-BDC MOFs were systematically studied to find the structure–activity relationship between the PET-derived ligand and supercapacitor performance. In addition, this work not only focuses on MOF design for energy storage but also provides an effective pathway for converting plastic waste into cheaper electrode materials, which contributes to environmental remediation and advanced energy technologies.

2. Experimental Section

2.1. Materials and Methods

Nickel(II) nitrate hexahydrate, N, N-dimethylformamide, ethanol, potassium hydroxide, sodium hydroxide, carbon black, polyvinylidene fluoride, N-methyl-2-pyrrolidone, hydrochloric acid, nitric acid, acetone, and isopropanol solution were purchased from Sigma-Aldrich, Bengaluru, India. These chemicals are of analytical grade and did not require further purification. We used double-distilled water throughout the experimental procedure. Waste plastic bottles were collected from garbage bins in and around Vellore, Tamil Nadu, India. The collected plastic bottles were cut into small pieces (approximately 1–2 cm^2), washed three times with deionized water to remove surface impurities, and oven-dried at 40 °C for 30 min before further use.

2.2. Extraction of Terephthalic Acid from PET Waste

Terephthalic acid (BDC) was synthesized by depolymerizing waste PET bottles via alkaline hydrolysis, as shown in Figure 1. A round-bottom flask equipped with a distillation chamber was used for the depolymerization reaction; 100 mL of 10% w/v sodium hydroxide solution was added to the RB flask, followed by 10 g of chopped PET flakes. The solution was heated and stirred continuously at 110 °C for 3 h. Afterward, a milky white solution was obtained and filtered to remove unreacted solids. Then, the solution pH was adjusted to 3 with concentrated hydrochloric acid to precipitate the BDC. After precipitation, BDC

was washed with deionized water and oven-dried at 80 °C for 12 h to remove moisture. The BDC yield was calculated using Equation (1).

$$Yield\ (\%) = \frac{m\ BDC}{0.865 \times [mPET]_0} \times 100 \quad (1)$$

where mBDC is the actual mass of recovered BDC (g) and $[mPET]_0$ is the initial mass of PET (g). The factor 0.865 is the theoretical weight fraction of BDC in the PET repeat unit [39].

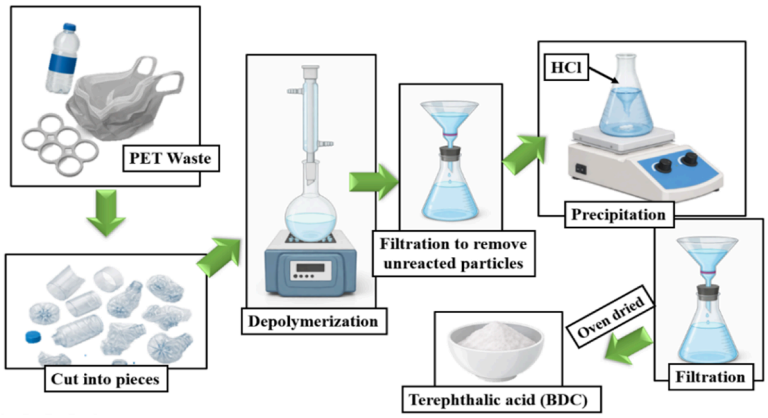


Figure 1. Alkaline hydrolysis of Waste PET bottles.

2.3. Synthesis of Nickel 1,4-Dicarboxylic Acid Frameworks (Ni-BDC MOF)

Ni-BDC MOF was prepared by simple co-precipitation (Figure 2); 1 g of Nickel (II) nitrate hexahydrate was diluted in double-distilled water, and 0.5 g of extracted BDC was dissolved in N, N-dimethylformamide, and sonicated continuously at room temperature until the particles were completely dissolved. The two solutions were mixed in a 100 mL beaker and stirred for 8 h. Afterward, the washed precipitate was filtered and centrifuged 3 times with ethanol to remove unreacted particles. The precipitate was transferred to a crucible and oven-dried at 110 °C for 12 h to remove water.

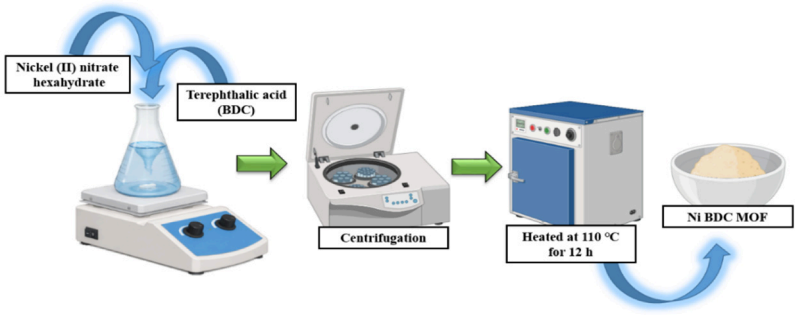


Figure 2. Ni-BDC MOF synthesis.

2.4. Characterization Techniques

The crystal phase of the material was characterized by X-ray diffraction (XRD, Bruker D8 Advance, Bruker AXS, Karlsruhe, Germany) using Cu-Kα radiation (λ = 1.5406 Å) at 40 kV and 40 mA. Fourier transform infrared (FTIR) spectra were recorded using a Nicolet iS50 spectrometer (Thermo Fisher Scientific, Madison, WI, USA) to identify the functional groups present in the samples. Surface morphology and microstructural properties were investigated using field-emission scanning electron microscopy (FE-SEM, Quanta 250 FEG, FEI Company, Hillsboro, OR, USA). Raman spectra were recorded using an XploRA Plus

Raman microscope (HORIBA France SAS, Palaiseau, France). UV–Visible absorption spectra were recorded on a V-770 spectrophotometer (JASCO Corporation, Tokyo, Japan) over 200–800 nm. X-ray photoelectron spectroscopy (XPS, VersaProbe 4, ULVAC-PHI, Inc., Chigasaki, Kanagawa, Japan) was employed to determine the surface chemical composition and oxidation states of the elements. The specific surface area and pore structure parameters were determined by N_2 adsorption–desorption analysis using a TriStar II surface area and porosity analyzer (Micromeritics Instrument Corporation, Norcross, GA, USA).

2.5. Electrochemical Measurements

The electrochemical behavior of the Ni-BDC MOF electrode was identified using cyclic voltammetry (CV), galvanostatic charge-discharge (GCD), and electrochemical impedance spectroscopy (EIS) on a Bio-Logic SP-200 workstation in a standard three-electrode setup. The platinum wire was used as the counter electrode, and an Ag/AgCl electrode was used as the reference. The working electrode was prepared from synthesized Ni-BDC MOF mixed with a polyvinylidene fluoride (PVDF) binder and a conductive additive, carbon black, at an 8:1:1 mass ratio. Carbon black was added to compensate for the MOF's limited intrinsic electronic conductivity and to improve electrical connectivity between MOF particles and electron transport through the electrode. N-Methyl-2-pyrrolidone (NMP) was added dropwise to form a uniform slurry, which was then coated onto a graphite sheet current collector (effective area: 1 cm^2). The coated electrode was dried at 80 °C for 8 h to evaporate the solvent. All tests were run in a 1 M KOH aqueous electrolyte at room temperature. EIS measurements were performed over a frequency range of 100 kHz to 100 mHz. Equation 2 was used to determine the electrode material's specific capacitance (Cm, F/g) from GCD curve data. Where I represents the discharge current (A) for the GCD test, Δt represents the discharge time (s) for the GCD test, m is the mass of the active material (g), and ΔV denotes the potential window (V) of the GCD test [40].

$$C_m = \frac{I \times \Delta t}{m \times \Delta v} \quad (2)$$

3. Results and Discussion

3.1. Characterization of Ni-BDC MOF

The structural, chemical, and morphological properties of the synthesized Ni-BDC MOF, which was obtained from the waste PET-based terephthalic acid (BDC), have been thoroughly examined using UV-Visible spectroscopy, Fourier transform infrared spectroscopy (FT-IR), X-ray diffraction (XRD), Raman spectroscopy, and scanning electron microscopy (SEM) analysis. These analyses confirm that Ni^{2+} ions have been successfully coordinated to the extracted organic linker. The yield of terephthalic acid was calculated by Equation (1). A yield of 7 g of dried terephthalic acid was obtained from 10 g of PET waste. Thus, the recovered terephthalic acid yield was 80.92%. The purity and structural integrity of the waste-derived terephthalic acid (W-TP) produced from PET depolymerization were first assessed and compared with commercial terephthalic acid (C-TP), as depicted in Figure 3a,b. The FT-IR spectra in Figure 3a indicate that W-TP has the same functional groups as C-TP. The broad O-H stretching region from 2500 to 3300 cm^{-1} and the strong C=O stretching vibration at approximately 1670 cm^{-1} indicate the presence of carboxylic acid functional groups in both W-TP and C-TP. The aromatic C=C stretching vibrations at 1410–1450 cm^{-1} and the C-H bending vibrations at 700–900 cm^{-1} further support the benzene ring structure. The W-TP spectrum shows no new impurity peaks, indicating that alkaline hydrolysis of PET successfully regenerated high-purity terephthalic acid with unaltered structural integrity [41–43]. Figure 3b shows the XRD patterns of waste

PET-derived terephthalic acid (W-TP) and commercial terephthalic acid (C-TP). The diffraction profiles were compared with previously reported XRD characteristics of terephthalic acid. Comparison of the experimental XRD patterns with the ICDD reference standard PDF No. 00-021-1919 showed good agreement in peak positions and relative intensities, confirming the characteristic crystalline features of terephthalic acid. The C-TP pattern shows well-resolved peaks indexed to the (110), (200), (211), and (220) planes, and similar features are observed in the W-TP pattern. Differences in relative peak intensities and profiles between the two samples may reflect differences in sample preparation and preferred crystallite orientation [44,45]. The diffraction peaks assigned to the (110), (200), and (211) planes were compared with previously reported Ni-BDC materials, showing similar diffraction features and supporting formation of the nickel terephthalate phase, with an average crystallite size of 24.07 nm [46–49]. The coordination interaction between Ni^{2+} ions and W-TP is confirmed using FT-IR spectra of the Ni-BDC MOFs (Figure 3e). The disappearance of the free carboxylic acid C=O stretching vibration at 1720 cm^{-1} and the appearance of the asymmetric and symmetric carboxylate stretching vibrations at 1630–1670 cm^{-1} and 1410–1450 cm^{-1}, clearly indicate the deprotonation and coordination of the carboxylate groups to Ni ions. The difference between the asymmetric and symmetric stretching vibrations indicates a bidentate bridging coordination mode. The appearance of Ni-O stretching vibrations below 700 cm^{-1} confirms the formation of metal-oxygen bonds. The Raman spectrum of the Ni-BDC MOF (Figure 3c) reveals characteristic aromatic bands, such as ring breathing at 830 cm^{-1}, C-H bending at 1120–1290 cm^{-1}, and prominent C=C stretching bands at 1446 and 1630 cm^{-1}. These bands indicate that the π-conjugated benzene framework is unaffected by the coordination reaction. This is important, as it ensures that the aromatic backbone of W-TP is not affected by depolymerization and coordination reactions [50]. The optical absorption spectrum shown in Figure 3f displays a prominent absorption edge at 240 nm, which is due to $\pi \rightarrow \pi^*$ transitions in the aromatic linker and possibly ligand-to-metal charge transfer (LMCT) transitions. The Tauc plot (Figure 4a) gives a band gap of approximately 4.6 eV, which falls within the band gap range of semiconducting materials. This suggests that the material lacks appreciable intrinsic electronic conductivity and that nickel redox sites and ion diffusion, mainly facilitated by electrochemical redox reactions, are present within the porous material. The surface morphology of the Ni-BDC MOF is presented in Figure 4b. The material has a stacked, rod-like, layered morphology with interconnecting domains. The rough surface morphology and hierarchical structure enhance surface area and provide multiple channels for electrolyte penetration. The surface morphology also provides an efficient interface for contact between the active sites and electrolyte ions, thus facilitating Faradaic reactions. The EDS analysis (Figure 4c) reveals Ni, C, and O, with no trace impurities. The absence of unwanted peaks evidences this. The elemental mapping images (Figure 4d) reveal a uniform distribution of Ni, C, and O. The uniform distribution of nickel in the organic framework indicates the absence of phase separation or metal aggregation, which is essential for stable electrochemical properties [51,52]. X-ray photoelectron spectroscopy (XPS) was used to analyze the chemical states and surface composition of the Ni-BDC MOF. The survey XPS (Figure 5a) revealed characteristic peaks of Ni (2p), C (1s), and O (1s), confirming the presence of Ni, C, and O. The C 1s spectrum (Figure 5b) shows peaks at 288.5, 285.3, and 284.8 eV corresponding to O–C=O, C–O, and C=C/C–C bonds, respectively. These peaks correspond to the carboxylate group and aromatic carbon framework of the BDC linker. The Ni 2p spectrum, which is shown in Figure 5c, has components, Ni $2p_{3/2}$ and Ni $2p_{1/2}$, around 855.6 and 873.6 eV, respectively. The O 1s spectrum displays peaks from Ni–O and carboxylate oxygen (Figure 5d). These peaks are assigned to oxygen from Ni and to oxygen in the functional groups present in the Ni-BDC MOF [38]. Figure 5e shows the nitrogen adsorption–desorption isotherm, which reveals a steady increase in nitrogen uptake with

increasing relative pressure. The BET analysis shows a specific surface area of 270.405 m^2 g^{-1}. Figure 6f shows the pore size distribution, which is dominated by 3.8-4.0 nm pores in the mesopore region [38]. These results indicate that terephthalic acid derived from waste PET (W-TP) has structural, crystalline, and chemical properties comparable to commercial terephthalic acid (C-TP). The ligand can bind Ni^{2+} ions to form a highly crystalline Ni-BDC MOF with bidentate carboxylate bridging. The preserved aromatic structure, crystallinity, uniform metal distribution, and appropriate morphology demonstrate W-TP's effectiveness as a green coordination ligand. This study shows that waste PET-derived terephthalic acid can be used directly as a precursor for synthesizing metal-organic frameworks without compromising structural integrity, offering a promising approach to converting plastic waste into a valuable functional coordination materials for energy storage applications.

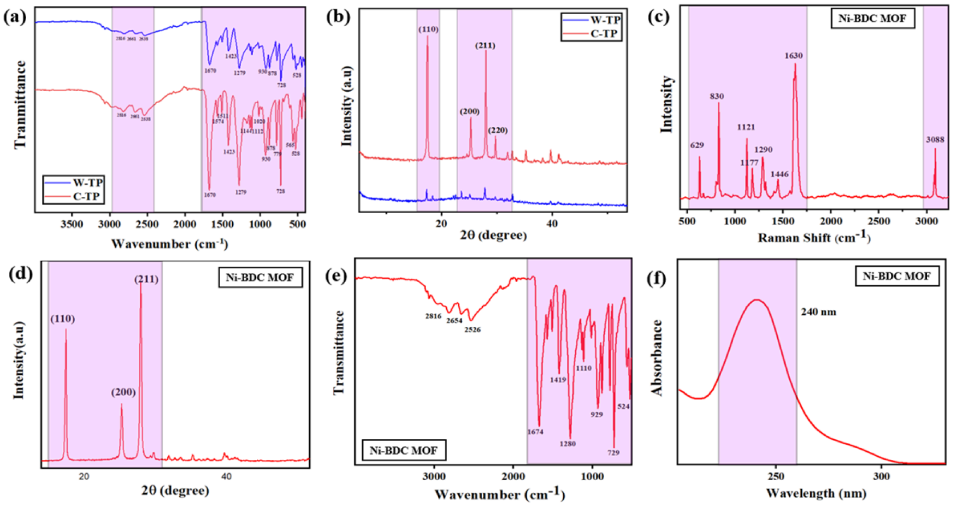


Figure 3. (**a**) FT-IR spectra of W-TP and C-TP; (**b**) XRD spectra of W-TP and C-TP; (**c**) Raman Spectra of Ni-BDC MOF; (**d**) XRD of Ni-BDC MOF; (**e**) FT-IR of Ni-BDC MOF; and (**f**) UV absorbance spectra of Ni-BDC MOF.

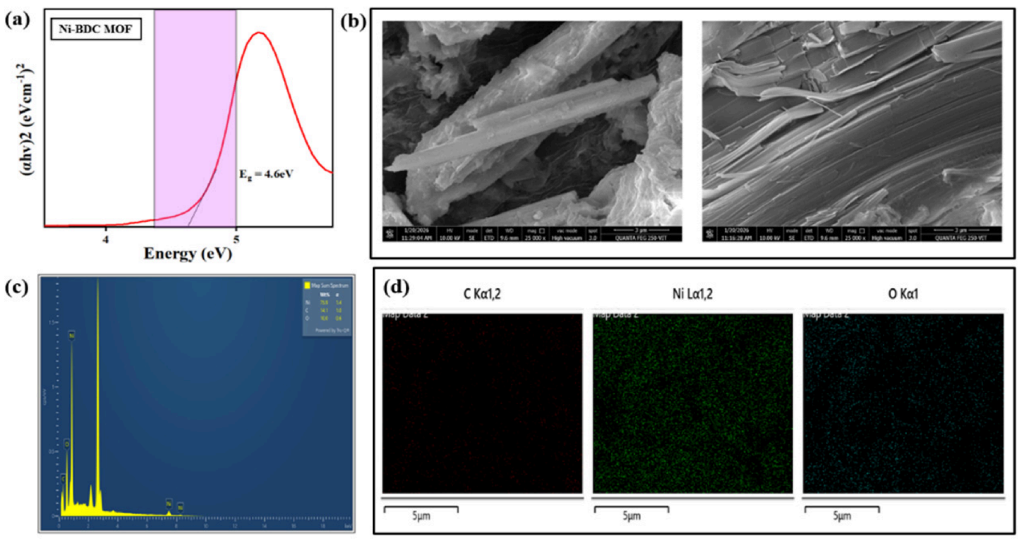


Figure 4. (**a**) Tauc plot of Ni-BDC MOF, (**b**) FE-SEM images of Ni-BDC MOF, (**c**) EDS spectrum of Ni-BDC MOF, and (**d**) elemental mapping of Ni-BDC MOF.

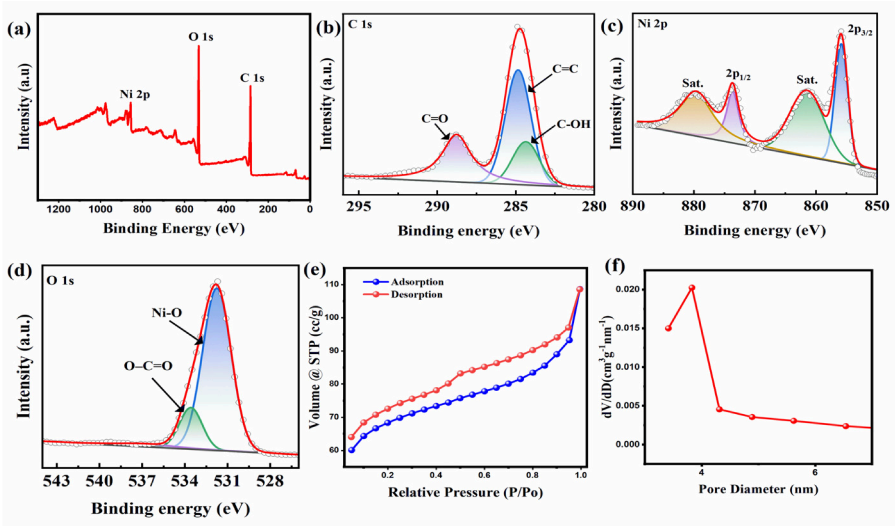


Figure 5. (**a**–**d**) XPS survey and high-resolution spectra of Ni-BDC MOF, (**e**) N_2 adsorption–desorption isotherm and (**f**) pore size distribution of Ni-BDC MOF.

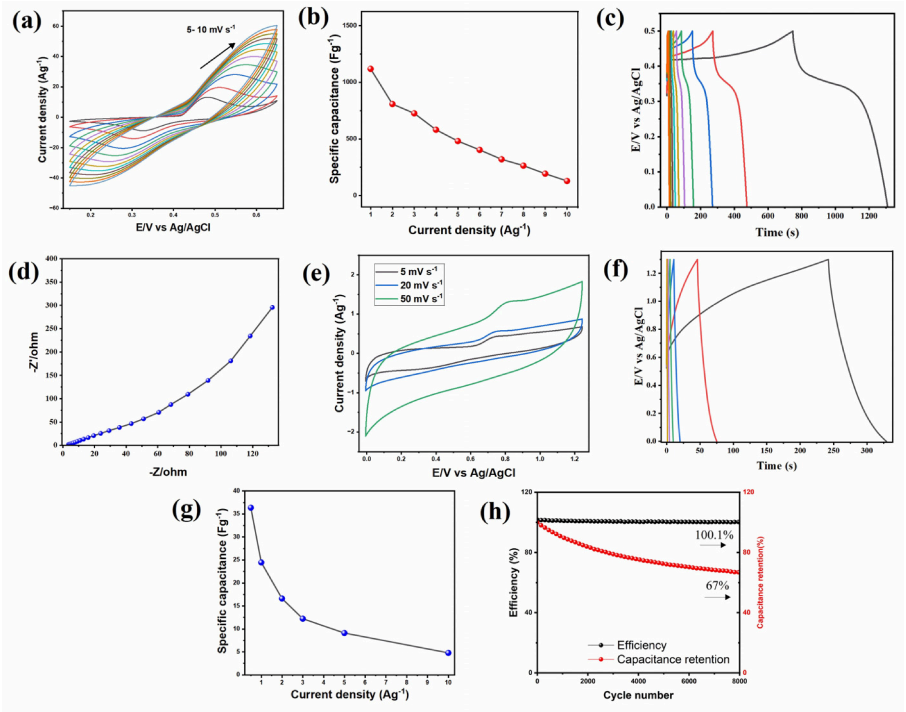


Figure 6. (**a**) Cyclic voltammetry (CV) curves of Ni-BDC MOF at different scan rates, (**b**) specific capacitance as a function of current density (Ni-BDC MOF), (**c**) galvanostatic charge-discharge (GCD) curves of Ni-BDC MOF, (**d**) Nyquist plot of Ni-BDC MOF, (**e**) CV curves of Ni-BDC MOF//KOH//Ni-BDC MOF, (**f**) GCD curves of Ni-BDC MOF//KOH//Ni-BDC MOF, (**g**) Specific capacitance as a function of current density (Ni-BDC MOF//KOH//Ni-BDC MOF), (**h**) cycling stability of Ni-BDC MOF at 15 A g^{-1} (8000 cycles).

3.2. Electrochemical Performance and Structure–Activity Relationship of Ni-BDC MOF

The electrochemical performance of Ni-BDC MOF was investigated using a three-electrode configuration and a symmetric two-electrode system to study charge-storage behavior, rate capability, impedance characteristics, and cycling stability [53,54]. The cyclic voltammetry (CV) curves of the Ni-BDC MOF electrode at different scan rates of 5–50 mV s^{-1} are shown in Figure 6a. The observed redox features suggest a Faradaic contribution to the charge-

storage mechanism. The increase in current response and CV curve area with increasing scan rate indicates a scan-rate-dependent electrochemical response. The specific capacitance values at different current densities are presented in Table 1 and Figure 6b. The Ni-BDC MOF electrode exhibited a specific capacitance of 1118 F g^{-1} at 1 A g^{-1}, which decreased to 808, 726, 581, 481, 403, 320, 264, 193, and 129 F g^{-1} at current densities of 2, 3, 4, 5, 6, 7, 8, 9, and 10 A g^{-1}, respectively. The corresponding galvanostatic charge-discharge (GCD) curves are presented in Figure 5c, where the discharge times at different current densities were used to calculate the specific capacitance. Figure 6d shows the Nyquist plot of the Ni-BDC MOF electrode. The solution resistance (Rs) was identified as 3.6 Ω from the high-frequency intercept on the real impedance axis. The predominantly inclined impedance response indicates non-ideal capacitive behavior and distributed charge-transport processes. We then evaluated the electrochemical performance of the symmetric two-electrode device, assembled with Ni-BDC MOF as both electrodes and 1 M KOH as the electrolyte (Ni-BDC MOF//1 M KOH//Ni-BDC MOF). Figure 6e shows the CV curves recorded at scan rates of 5, 20, and 50 mV s^{-1}. The increased current response with increasing scan rate demonstrates the device's rate-dependent charge-storage behavior. Corresponding GCD curves at different current densities are presented in Figure 6f. The symmetric device showed specific capacitances of 36.36, 24.47, 16.63, 12.25, 9.16, and 4.83 F g^{-1} at current densities of 0.5, 1, 2, 3, 5, and 10 A g^{-1}, respectively (Table 2 and Figure 6g). The decline in specific capacitance with increasing current density can be attributed to hindered electrolyte-ion diffusion and reduced accessibility of the electroactive sites during fast charge-discharge processes. These results demonstrate the current-density-dependent charge-storage performance of the symmetric device. The cycling stability of the symmetric Ni-BDC MOF//1 M KOH//Ni-BDC MOF device was evaluated over 8000 consecutive GCD cycles at a constant current density of 15 A g^{-1}, as shown in Figure 6h. Capacitance retention was evaluated by comparing the specific capacitance of the first GCD cycle with that of the 8000th cycle. Under the applied conditions, the device showed moderate long-term cycling stability, retaining 67% of the initial capacitance over 8000 cycles. The coulombic efficiency reached 100.1%, indicating good charge-discharge reversibility during cycling. This long-term cycling-induced capacitance loss may relate to changes at the electrode/electrolyte interface or reduced availability of electroactive sites. Overall, the results demonstrate Ni-BDC MOF's electrochemical charge-storage capability in both three-electrode and symmetric two-electrode configurations. In contrast, the cycling results establish its stability over 8000 GCD cycles.

Table 1. Specific capacitance as a function of current density (Ni-BDC MOF).

S.NO.	Current Density (A/g)	Specific Capacitance (Fg^{-1})
1.	1	1118
2.	2	808
3.	3	726
4.	4	581
5.	5	481
6.	6	403
7.	7	320
8.	8	264
9.	9	193
10.	10	129

Table 2. Specific capacitance as a function of current density (Ni-BDC MOF//KOH//Ni-BDC MOF).

S.NO.	Current Density (A/g)	Specific Capacitance (Fg^{-1})
1.	0.5	36.36
2.	1	24.47
3.	2	16.63
4.	3	12.25
5.	5	9.16
6.	10	4.83

4. Conclusions

The Ni-BDC MOF was synthesized from terephthalic acid derived from waste PET, and its electrochemical performance was evaluated in a three-electrode and symmetric two-electrode configuration. The structural, morphological, and surface chemical properties were investigated using XRD, FTIR, Raman spectroscopy, FE-SEM, XPS, and BET analyses, which confirmed the formation of Ni-BDC MOF. Three-electrode measurements showed a specific capacitance of 1118 F g^{-1} at 1 Ag^{-1}, which decreased to 129 F g^{-1} at 10 Ag^{-1}, suggesting that capacitance decreases with increasing current density. Electrochemical impedance spectroscopy showed a solution resistance (R_s) of 3.6 Ω and a mostly inclined Nyquist response, suggesting non-ideal capacitive behavior. The symmetric two-electrode device in 1 M KOH exhibited a specific capacitance of 36.36 F g^{-1} at 0.5 Ag^{-1} and 4.83 F g^{-1} at 10 Ag^{-1}. The cycling stability was tested at 15 $Ag^{-1,}$ and about 67% capacitance retention was obtained after 8000 galvanostatic charge-discharge cycles with about 100.1% coulombic efficiency. This work links recycling waste PET with the development of Ni-BDC MOF electrode materials. It highlights the potential of using plastic-waste-derived terephthalic acid for energy storage applications and contributes to circular-economy efforts.

Author Contributions: Conceptualization, M.P. and D.T.; formal analysis, D.D.; Investigation, conceptualization, and methodology, D.D. D.D. and S.D.; writing—original draft preparation, R.J. and J.T.; writing—review and editing, M.P., D.T. and J.T.; visualization, R.J. and P.R.K.; supervision. All authors have read and agreed to the published version of the manuscript.

Funding: This research received no external funding.

Data Availability Statement: The data supporting the findings of this study are available from the corresponding author upon reasonable request.

Acknowledgments: The authors thank the CO_2 RGTC, Vellore Institute of Technology, Vellore-632014, India, for providing the necessary research facilities to carry out this work. Furthermore, the authors extend their sincere gratitude to Cracow University of Technology, Poland, for its valuable technical support and research collaboration throughout this study.

Conflicts of Interest: The authors declare no conflicts of interest.

References

1. Zeng, Q.; Li, C.; Magazzino, C. Impact of Green Energy Production for Sustainable Economic Growth and Green Economic Recovery. *Heliyon* **2024**, *10*, e36643. [CrossRef] [PubMed]
2. Prasankumar, T.; Manoharan, K.; Farhana, N.K.; Bashir, S.; Ramesh, K.; Ramesh, S.; Ramachandaramurthy, V.K. Advancements and Approaches in Developing MXene-Based Hybrid Composites for Improved Supercapacitor Electrodes. *Mater. Today Sustain.* **2024**, *28*, 100963. [CrossRef]
3. Zhang, J. Energy Access Challenge and the Role of Fossil Fuels in Meeting Electricity Demand: Promoting Renewable Energy Capacity for Sustainable Development. *Geosci. Front.* **2024**, *15*, 101873. [CrossRef]

4. Perera, F. Pollution from Fossil-Fuel Combustion Is the Leading Environmental Threat to Global Pediatric Health and Equity: Solutions Exist. *Int. J. Environ. Res. Public Health* **2017**, *15*, 16. [CrossRef] [PubMed]
5. Islam, M.K.; Hassan, N.M.S.; Rasul, M.G.; Emami, K.; Chowdhury, A.A. Green and Renewable Resources: An Assessment of Sustainable Energy Solution for Far North Queensland, Australia. *Int. J. Energy Environ. Eng.* **2023**, *14*, 841–869. [CrossRef]
6. Ang, T.-Z.; Salem, M.; Kamarol, M.; Das, H.S.; Nazari, M.A.; Prabaharan, N. A Comprehensive Study of Renewable Energy Sources: Classifications, Challenges and Suggestions. *Energy Strategy Rev.* **2022**, *43*, 100939. [CrossRef]
7. Abbas, Q.; Mirzaeian, M.; Hunt, M.R.C.; Hall, P.; Raza, R. Current State and Future Prospects for Electrochemical Energy Storage and Conversion Systems. *Energies* **2020**, *13*, 5847. [CrossRef]
8. Zhang, J.; Gu, M.; Chen, X. Supercapacitors for Renewable Energy Applications: A Review. *Micro Nano Eng.* **2023**, *21*, 100229. [CrossRef]
9. Iqbal, M.F.; Nasir, F.; Shabbir, F.; Babar, Z.U.D.; Saleem, M.F.; Ullah, K.; Sun, N.; Ali, F. Supercapacitors: An Emerging Energy Storage System. *Adv. Energy Sustain. Res.* **2025**, *6*, 2400412. [CrossRef]
10. Winter, M.; Brodd, R.J. What Are Batteries, Fuel Cells, and Supercapacitors? *Chem. Rev.* **2003**, *104*, 4245–4269. Correction in *Chem. Rev.* **2005**, *105*, 1021. https://doi.org/10.1021/cr040110e. [CrossRef] [PubMed]
11. Lobato-Peralta, D.R.; Alegre, C.; Okolie, J.A.; Okoye, P.U. Batteries, Capacitors and Supercapacitors: Comparative Analysis and Advantages for Storing Electrical Energy. In *Supercapacitors*; Verma, D.K., Aslam, J., Eds.; Royal Society of Chemistry: London, UK, 2025; pp. 454–492.
12. Sharma, S.; Chand, P. Supercapacitor and Electrochemical Techniques: A Brief Review. *Results Chem.* **2023**, *5*, 100885. [CrossRef]
13. Zhang, W.; Sun, C.; Alharbi, M.; Hasanien, H.M.; Song, K. A Voltage-Power Self-Coordinated Control System on the Load-Side of Storage and Distributed Generation Inverters in Distribution Grid. *Ain Shams Eng. J.* **2025**, *16*, 103480. [CrossRef]
14. Yue, T.; Shen, B.; Gao, P. Carbon Material/MnO_2 as Conductive Skeleton for Supercapacitor Electrode Material: A Review. *Renew. Sustain. Energy Rev.* **2022**, *158*, 112131. [CrossRef]
15. Tundwal, A.; Kumar, H.; Binoj, B.J.; Sharma, R.; Kumar, G.; Kumari, R.; Dhayal, A.; Yadav, A.; Singh, D.; Kumar, P. Developments in Conducting Polymer-, Metal Oxide-, and Carbon Nanotube-Based Composite Electrode Materials for Supercapacitors: A Review. *RSC Adv.* **2024**, *14*, 9406–9439. [CrossRef] [PubMed]
16. Balasubramaniam, S.; Mohanty, A.; Balasingam, S.K.; Kim, S.J.; Ramadoss, A. Comprehensive Insight into the Mechanism, Material Selection and Performance Evaluation of Supercapatteries. *Nano-Micro Lett.* **2020**, *12*, 85. [CrossRef] [PubMed]
17. Choi, Y.-S.; Costa, S.I.R.; Tapia-Ruiz, N.; Scanlon, D.O. Intrinsic Defects and Their Role in the Phase Transition of Na-Ion Anode $Na_2Ti_3O_7$. *ACS Appl. Energy Mater.* **2023**, *6*, 484–495. [CrossRef] [PubMed]
18. Li, S.; Luo, J.; Wang, J.; Zhu, Y.; Feng, J.; Fu, N.; Wang, H.; Guo, Y.; Tian, D.; Zheng, Y.; et al. Hybrid Supercapacitors Using Metal-Organic Framework Derived Nickel-Sulfur Compounds. *J. Colloid Interface Sci.* **2024**, *669*, 265–274. [CrossRef] [PubMed]
19. Ferhi, N.; Desalegn Assresahegn, B.; Ardila-Suarez, C.; Dissem, N.; Guay, D.; Duong, A. Defective Metal–Organic Framework-808@Polyaniline Composite Materials for High Capacitance Retention Supercapacitor Electrodes. *ACS Appl. Energy Mater.* **2022**, *5*, 1235–1243. [CrossRef]
20. Han, Z.; Yang, Y.; Rushlow, J.; Huo, J.; Liu, Z.; Hsu, Y.-C.; Yin, R.; Wang, M.; Liang, R.; Wang, K.-Y.; et al. Development of the Design and Synthesis of Metal–Organic Frameworks (MOFs)—From Large Scale Attempts, Functional Oriented Modifications, to Artificial Intelligence (AI) Predictions. *Chem. Soc. Rev.* **2025**, *54*, 367–395. [CrossRef] [PubMed]
21. Argirusis, C.; Katsanou, M.-E.; Alizadeh, N.; Argirusis, N.; Sourkouni, G. Recent Advances in the Application of MOFs in Supercapacitors. *Batteries* **2025**, *11*, 181. [CrossRef]
22. Ansari, M.Z.; Habib, F.; Gupta, J.; Alsubaie, A.S.; Barsoum, I.; Alfantazi, A.; Yatoo, M.A.; Ahmad, Z.; Hussain, I. Frontiers in Metal–Organic Frameworks: Innovative Nanomaterials for next-Generation Supercapacitors. *Adv. Compos. Hybrid Mater.* **2024**, *7*, 215. [CrossRef]
23. Raikwar, A.S.; Panda, H.S. A Review on Nano-Structured Electrodes for High-Performance Supercapacitors: Panoramic Insights across Dimensional Spectra. *Discov. Electron.* **2025**, *2*, 94. [CrossRef]
24. Ramulu, B.; Yu, J.S. Recent Advances in Metal-Organic Frameworks-Based Materials for Supercapacitor Applications. *Appl. Sci. Converg. Technol.* **2024**, *33*, 53–61. [CrossRef]
25. Makgopa, K.; Ratsoma, M.S.; Modibane, K.D. Intrinsic Properties of Metal–Organic Frameworks (MOFs) in Supercapacitor Applications. *Curr. Opin. Electrochem.* **2022**, *36*, 101112. [CrossRef]
26. Sahoo, M.K.; Mane, P.; Chakraborty, B.; Behera, J.N. Three-Dimensional Ni-MOF as a High-Performance Supercapacitor Anode Material; Experimental and Theoretical Insight. *Inorg. Chem.* **2024**, *63*, 6383–6395. [CrossRef] [PubMed]
27. Jin, X.; Jiang, Z.; Feng, Y.; Fang, X. Optimization of Cobalt-Based MOFs for Super-Capacitor Electrode Materials of New Energy Vehicle. *Heliyon* **2024**, *10*, e31222. [CrossRef] [PubMed]
28. Chen, L.-D.; Zheng, Y.-Q.; Zhu, H.-L. Manganese Oxides Derived from Mn(II)-Based Metal–Organic Framework as Supercapacitor Electrode Materials. *J. Mater. Sci.* **2018**, *53*, 1346–1355. [CrossRef]

29. Liu, X.-H.; Jia, X.-L.; Zhao, Y.-L.; Zheng, R.-X.; Meng, Q.-L.; Liu, C.-P.; Xing, W.; Xiao, M.-L. Recent Advances in Nickel-Based Catalysts for Electrochemical Reduction of Carbon Dioxide. *Adv. Sens. Energy Mater.* **2023**, *2*, 100073. [CrossRef]
30. Manzoor, F.; Majeed, A.; Ibrahim, A.H.; Iqbal, M.A.; Rehman, A.; Aziz, S.; Shahzadi, A.; Fatima, S.; Ejaz, S.; Zafar, M.S. Nickel-Photoredox Catalysis: Merging Photons with Metal Catalysts for Organic Synthesis. *RSC Adv.* **2025**, *15*, 33345–33364. [CrossRef]
31. Xiang, Y.; Wei, S.; Wang, T.; Li, H.; Luo, Y.; Shao, B.; Wu, N.; Su, Y.; Jiang, L.; Huang, J. Transformation of Metal-Organic Frameworks (MOFs) under Different Factors. *Coord. Chem. Rev.* **2025**, *523*, 216263. [CrossRef]
32. Abdelhameed, R.M.; El-Shahat, M. The Role of Carboxylic Acid Contents in Calcium-Based Metal-Organic Frameworks for the Enhancement of Biginelli Reaction. *J. Mol. Struct.* **2025**, *1321*, 139742. [CrossRef]
33. Biswas, A.; Kim, M.-B.; Kim, S.-Y.; Yoon, T.-U.; Kim, S.-I.; Bae, Y.-S. A Novel 3-D Microporous Magnesium-Based Metal–Organic Framework with Open Metal Sites. *RSC Adv.* **2016**, *6*, 81485–81490. [CrossRef]
34. Rastin, H.; Dell'Angelo, D.; Sayede, A.; Badawi, M.; Habibzadeh, S. Green and Sustainable Metal-Organic Frameworks (MOFs) in Wastewater Treatment: A Review. *Environ. Res.* **2025**, *282*, 122087. [CrossRef] [PubMed]
35. Babaei, M.; Jalilian, M.; Shahbaz, K. Chemical Recycling of Polyethylene Terephthalate: A Mini-Review. *J. Environ. Chem. Eng.* **2024**, *12*, 112507. [CrossRef]
36. Wang, Y.; Wang, H.; Li, S.; Sun, S. Waste PET Plastic-Derived CoNi-Based Metal–Organic Framework as an Anode for Lithium-Ion Batteries. *ACS Omega* **2022**, *7*, 35180–35190. [CrossRef] [PubMed]
37. Silerio-Vázquez, F.D.J.; Hosseini-Bandegharaei, A.; Abdikalykov, R.; Baigenzhenov, O.; Kakavandi, B.; Robledo-Peralta, A. Recycled PET-Derived MOF for Photocatalytic Degradation of Emerging Pollutants: Recent Progress and Critical Considerations. *Environ. Res.* **2026**, *288*, 123231. [CrossRef] [PubMed]
38. Wei, L.; Wang, R.; Zhao, L.; Ren, Z.; Bai, H.; Zhang, Z.; Ju, Y.; He, Y. Preparation of Ni-MOFs Supercapacitor Electrode Materials Based on Benzene Carboxylic Acid Derivative Ligands and Their Structure-Activity Relationship. *J. Solid State Electrochem.* **2026**, *30*, 1535–1547. [CrossRef]
39. Muthubi, S.; Mwenge, P.; Tsolekile, N.; Mabuza, M. Alkaline Hydrolysis Depolymerisation of Waste Polyethylene Terephthalate (PET): Optimisation, ANN, ANFIS, and Kinetic Study. *Arab. J. Sci. Eng.* **2026**, *51*, 22381–22401. [CrossRef]
40. Govindarajan, D.; Palaniyandy, N.; Chinnakutti, K.K.; Nguyen, M.T.; Yonezawa, T.; Qin, J.; Kheawhom, S. Sputter-Deposited Binder-Free Nanopyramidal Cr/γ-Mo2N TFEs for High-Performance Supercapacitors. *Nanoscale Res. Lett.* **2022**, *17*, 65. [CrossRef] [PubMed]
41. Akkinepally, B.; Kumar, G.D.; Reddy, I.N.; Rao, H.J.; Nagajyothi, P.C.; Alothman, A.A.; Alqahtani, K.N.; Hassan, A.M.; Javed, M.S.; Shim, J. Investigation of Supercapacitor Electrodes Based on MIL-101(Fe) Metal-Organic Framework: Evaluating Electrochemical Performance through Hydrothermal and Microwave-Assisted Synthesis. *Crystals* **2023**, *13*, 1547. [CrossRef]
42. Chaturvedi, G.; Jaiswal, R.; Ilangovan, S.A.; Sujatha, S.; Ajeesh, K.S.; Tatiparti, S.S.V. Ni-MOF Based Flexible Solid-State Supercapacitors in Aqueous and Non-Aqueous Electrolytes. *ECS Meet. Abstr.* **2023**, *MA2023-02*, 13. [CrossRef]
43. Onwucha, C.N.; Ehi-Eromosele, C.O.; Ajayi, S.O.; Schaefer, M.; Indris, S.; Ehrenberg, H. Uncatalyzed Neutral Hydrolysis of Waste PET Bottles into Pure Terephthalic Acid. *Ind. Eng. Chem. Res.* **2023**, *62*, 6378–6385. [CrossRef]
44. Cosimbescu, L.; Merkel, D.R.; Darsell, J.; Petrossian, G. Simple But Tricky: Investigations of Terephthalic Acid Purity Obtained from Mixed PET Waste. *Ind. Eng. Chem. Res.* **2021**, *60*, 12792–12797. [CrossRef]
45. Tabassum, S.; Debnath, P.; Farid Ahmed, M.d.; Shahriar Bashar, M.; Akhtar, U.S.; Ahmed, S.; Sahadat Hossain, M.d. Sustainable Synthesis of Ni-Based Metal–Organic Framework from Waste Plastic as a Potential Electrochemical Sensor for Detecting Heavy Metals. *ACS Sustain. Resour. Manag.* **2026**, *3*, 1097–1111. [CrossRef]
46. Ehi-Eromosele, C.O.; Ajayi, S.O.; Nwaturuocha, C.N.; Talabi, J.O. Synthesis of Cu/Ni-Based Metal Organic Frameworks from Waste PET Bottles for Wastewater Treatment. *Results Chem.* **2025**, *16*, 102454. [CrossRef]
47. Zhao, Y.; Li, D.; Cai, P.; Ni, X.; Chen, G.; Xia, D.; Sun, Z.; Yuan, H. Architectural Modulation of Binary Metal-Organic Frameworks Upcycled from Waste Polyethylene Terephthalate for High-Performance Supercapacitors. *J. Colloid Interface Sci.* **2025**, *700*, 138666. [CrossRef] [PubMed]
48. Song, K.; Qiu, X.; Han, B.; Liang, S.; Lin, Z. Efficient Upcycling Electroplating Sludge and Waste PET into Ni-MOF Nanocrystals for the Effective Photoreduction of CO_2. *Environ. Sci. Nano* **2021**, *8*, 390–398. [CrossRef]
49. Manamela, L.; Nombona, N. Influence of Copper and Nickel Nodes on the Adsorption Behavior of Metal Organic Framework Cellulose Nanocrystal and Acetate Composite Films. *Discov. Polym.* **2026**, *3*, 28. [CrossRef]
50. Zakari, R.S.B.; Raj, A.; Hassan Ali, M.I.; Elkadi, M. One-Pot Synthesis of 2D-Ni-MOF from Waste PET Plastic in Aqueous Medium for Selective Electrooxidation of Glycerol, Ethanol, and Methanol. *J. Environ. Chem. Eng.* **2024**, *12*, 114542. [CrossRef]
51. Haris Azhar, M.; Noor, T.; Iqbal, N.; Zaman, N.; Farrukh, S. CO_2 Adsorption Properties of Ni-BDC MOF and Its 1–8 Wt% g-C3N4/Ni-BDC MOF. *Mater. Sci. Eng. B* **2024**, *299*, 117043. [CrossRef]
52. Elshafei, M.F.; Mostafa, M.R.; Khalf-Alla, P.A.; Mohamed, G.G.; Fouad, O.A. Kinetic and Isotherm Study of Ni-MOF/Magnetite Nanoparticles Adsorption Capacity as Green Synthesized Adsorbent towards Rhodochrome (Kammererite). *Sci. Rep.* **2025**, *15*, 44669. [CrossRef] [PubMed]

53. Zhou, D.; Ni, J. Ligand Engineering Toward Robust Sodium Storage in Self-Supported Metal-Organic Frameworks. *Chem.-Eur. J.* **2025**, *31*, e202403902. [CrossRef] [PubMed]
54. Alipour, A.H.; Lashkenari, M.S.; Ghorbani, M.; Kafshgari, L.A. In-Situ Growth of NiS-Ni_3S_4 on Dual-Ligand Co-MOF as a New Electrode for High-Performance Supercapacitors. *Sci. Rep.* **2025**, *15*, 39075. [CrossRef] [PubMed]

Disclaimer/Publisher's Note: The statements, opinions and data contained in all publications are solely those of the individual author(s) and contributor(s) and not of MDPI and/or the editor(s). MDPI and/or the editor(s) disclaim responsibility for any injury to people or property resulting from any ideas, methods, instructions or products referred to in the content.